ACS NANO

www.acsnano.org

ARTICLE

DNA-Tetrahedral-Nanostructure-Based Entropy-Driven Amplifier for High-Performance Photoelectrochemical Biosensing

Hongbo Li,* Min Han, Xuan Weng, Yuye Zhang, and Jing Li*

Cite This: *ACS Nano* 2021, 15, 1710–1717

Read Online

ACCESS | Metrics & More | Article Recommendations | Supporting Information

ABSTRACT: In virtue of the inherent molecular recognition and programmability, DNA has recently become the most promising for high-performance biosensors. The rationally engineered nucleic acid architecture will be very advantageous to hybridization efficiency, specificity, and sensitivity. Herein, a robust and split-mode photoelectrochemical (PEC) biosensor for miRNA-196a was developed based on an entropy-driven tetrahedral DNA (EDTD) amplifier coupled with superparamagnetic nanostructures. The DNA tetrahedron structure features in rigidity and structural stability that contribute to obtain precise identification units and specific orientations, improving the hybridization efficiency, sensitivity, and selectivity of the as-designed PEC biosensor. Further, superparamagnetic Fe_3O_4@SiO_2@CdS particles integrated with DNA nanostructures are beneficial for the construction of a split-mode, highly selective, and reliable PEC biosensor. Particularly, the enzyme- and hairpin-free EDTD amplifier eliminates unnecessary interference from the complex secondary structure of pseudoknots or kissing loops in typical hairpin DNAs, significantly lowers the background noise, and improves the detection sensitivity. This PEC biosensor is capable of monitoring miRNA-196a in practical settings with additional advantages of efficient electrode fabrication, stability, and reproducibility. This strategy can be extended to various miRNA assays in complex biological systems with excellent performance.

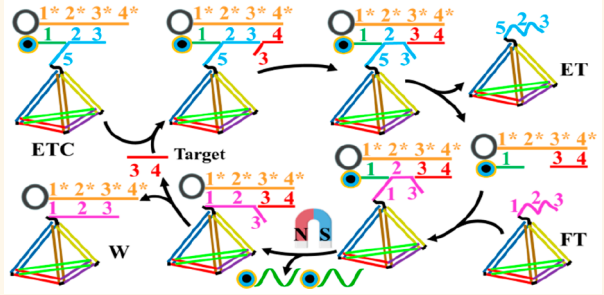

KEYWORDS: *entropy-driven amplifier, DNA tetrahedron, superparamagnetism, biosensing, microRNAs*

DNA has the advantages of superior controllability, programmability, and high precision.[1] Thanks to the development of DNA nanotechnology, DNA nanostructures can be constructed from the bottom up and assembled with various shapes and structures. A rationally engineered nucleic acid architecture will be very advantageous to hybridization efficiency, specificity, and sensitivity for biosensors.[2] Comparatively speaking, hairpin DNA is probably the most famous of various nucleic acid structures applied in biosensors because it helps to improve specificity and sensitivity. Therefore, this architecture has been paired with a variety of signal outputs such as fluorescent,[3] electrochemical,[4] and colorimetric readouts.[5] In order to achieve enhanced sensitivity, DNA-hairpin-architecture-based signal amplification strategies such as hybridization chain reaction (HCR),[6] catalytic hairpin assembly (CHA),[7] and rolling circle amplification (RCA)[8] have been developed for challenging miRNA detection or imaging. These amplification strategies really improve detection sensitivity. However, they still suffer from some shortcomings such as the probable demand for enzymes (RCA, for example), the high background noise, the side reactions, and false positive signals,[9] thus leading to high cost and limited sensitivity, specificity, or reliability. Alternatively, other than the two-dimensional hairpin DNA, in the past decade, three-dimensional tetrahedron DNA (THD) has attracted the attention of chemists mainly because of its favorable regulation of DNA hybridization,[10] supermolecular compact nature via intercalation,[11] good cell permeation, and high resistance to enzymatic degradation.[12] With mechanical rigidity, nanoscale addressing capability, and versatility in hand,

Received: November 9, 2020
Accepted: January 8, 2021
Published: January 13, 2021

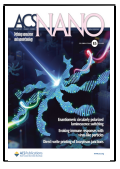

https://dx.doi.org/10.1021/acsnano.0c09374
ACS Nano 2021, 15, 1710–1717

Scheme 1. Assembly of the ETC Module (A) and the FT Module (B); (C) Schematic Illustration of Entropy-Driven Amplifier-Based Signal-on PEC Biosensing

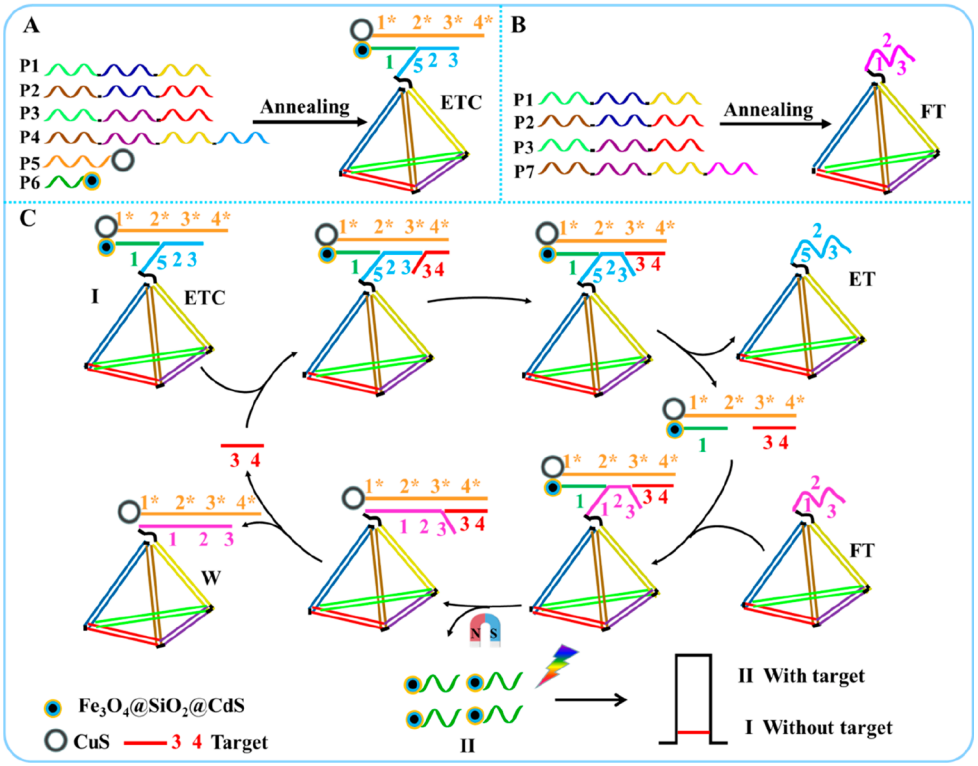

THD has special orientation and high hybridization efficiency, which has been applied in single nucleotide polymorphisms,[13] single molecular detection,[14] multiplex detection,[15,16] and size-selective molecular recognition,[17] greatly benefiting the sensitivity and specificity of biosensors. Compared with single-stranded aptasensors, the sensitivity of THD-assisted biosensors can be increased by more than 2 orders of magnitude.[18] Therefore, THD-based biosensors that are coupled with various signal expressions such as electrochemistry,[10] fluorescence,[12] colorimetry,[19] and electrochemiluminescence (ECL)[20] have been proposed. Similar to the separation of signal excitation and acquisition for ECL, in the past decade, photoelectrochemical (PEC) sensors have witnessed rapid development owing to their ultrasensitive features. For example, Yuan and co-workers developed a near-zero background and THD-assisted PEC biosensor for microRNA-141 (miRNA-141).[21] Nevertheless, on one hand, the duplex specific nuclease was demanded for signal multiplication; on the other hand, THD was only utilized as the nanocarrier, disregarding its great merits in recognition and hybridization. Therefore, a real enzyme- and hairpin-free THD-based PEC biosensor with high performance will hold great potential for miRNA measurement in practical applications.

Abnormally expressed miRNAs have become indicators of cancer diagnosis.[22,23] So far, several traditional strategies have been introduced including Northern blotting,[24] microarrays,[25] and quantitative RT-PCR.[26,27] These approaches contribute to their respective strengths such as good specificity, high throughput, and high accuracy. However, they are still limited in sensitivity and cost-effectiveness and typically require large amounts of RNA samples and are time-consuming. Obviously, for the challenging detection of low-abundance miRNAs, it is typically essential to employ unconventional strategies to amplify signal. In 2007, the Winfree group proposed a pioneering entropy-driven strategy that established a theoretical basis for the operation of DNA molecular machines.[28] Since the operation of molecular machines is nothing but the process of DNA hybridization and DNA strand displacement, introducing the THD structure with excellent hybridization recognition efficiency into the entropy-driven molecular machine will undoubtedly make the two complement each other, thus further improving the detection sensitivity and specificity of biosensors. Recently, Tan and co-workers developed an enzyme- and hairpin-free entropy-driven tetrahedral DNA (EDTD) amplifier for ultrasensitive fluorescent detection of miRNA.[12] Also, the Chen group reported a miRNA PEC biosensor by an entropy-driven amplifier coupled with magnetic beads.[29] Although with high selectivity and ultrasensitivity, this energy-transfer-based PEC biosensor still does not circumvent tedious electrode assembly. Aiming at simplifying the electrode assembly and constructing biosensors with high sensitivity, excellent specificity, as well as good stability and reproducibility, superparamagnetic nanoarchitectures are essential.[30] Obviously, integrating EDTD amplifiers with superparamagnetic nanoarchitectures into a PEC biosensing platform is very promising.

Herein, an enzyme- and hairpin-free robust PEC biosensor for miRNA-196a was constructed by an EDTD amplifier integrated to superparamagnetic nanostructures. As shown in Scheme 1, before initiation by targets, the photocurrent from the CdS shell layer is suppressed because the CuS hollow sphere as a blocking element competitively captures the incoming photons. The initiation of target by toehold-mediated strand displacement enables the separation of the Fe_3O_4@SiO_2@CdS composite and the blocker, restoring the

https://dx.doi.org/10.1021/acsnano.0c09374
ACS Nano 2021, 15, 1710−1717

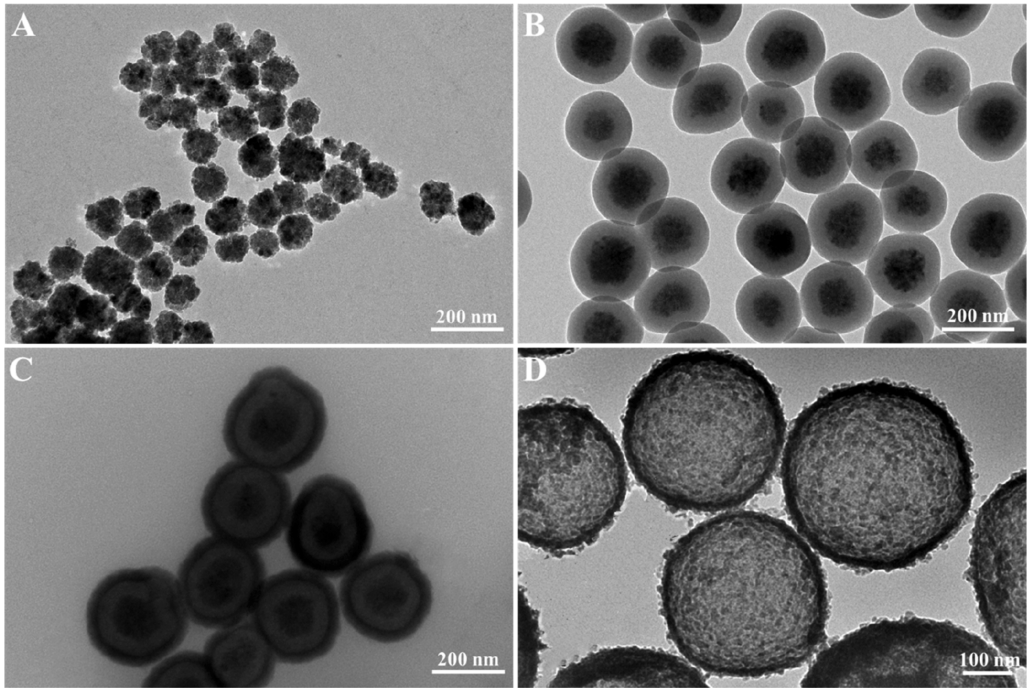

Figure 1. HRTEM images of Fe_3O_4 (A), Fe_3O_4@SiO_2 (B), Fe_3O_4@SiO_2@CdS (C), and CuS (D) particles.

photocurrent. Benefiting from the superparamagnetic property of the magnetic-optical beacon, the target recognition could be completed in the liquid phase, and the photocurrent could be acquired after magnetic separation, redispersion, and modification onto indium−tin oxide (ITO) electrodes. Based on this working mechanism, this signal-on and split-mode PEC biosensor is capable of monitoring miRNA-196a in practical settings with good performance in sensitivity, specificity, stability, and reproducibility. Particularly, this exclusive THD-assisted entropy-driven amplifier exhibits improved mechanical rigidity and biostability in contrast to those conventional entropy-driven ones.[12] Also, the EDTD amplifier is driven forward thermodynamically. During this process, the amount of base pairs remains constant, which is advantageous over the hairpin-based designs in reaction speed, stability, and sensitivity. Also, it can eliminate the unnecessary background interference caused by the complex secondary structure of pseudoknots or kissing loops in hairpin DNAs.[28] This work proposes an idea for the construction of high-performance miRNA biosensors in complex systems.

RESULTS AND DISCUSSION

Material Characterizations. The configurations and microscopic structures of the prepared nanomaterials were carried out by high-resolution transmission electron microscopy (HRTEM) imaging. Figure 1A shows that the size of the Fe_3O_4 colloidal nanocrystal clusters is approximately 95 nm, which is composed of ∼10 nm Fe_3O_4 nanocrystals. After coating of SiO_2, the resulting Fe_3O_4@SiO_2 particles noticeably show smooth surfaces with a size of ∼175 nm (Figure 1B). After further coating of CdS, the size of the core−shell−shell structure is increased to ∼215 nm, suggesting the achievement of Fe_3O_4@SiO_2@CdS particles. Also, the well-contoured CuS hollow microspheres with a size of ∼250 nm are shown in Figure 1D. The multicolor patterns of elemental mapping individually correspond to Fe_3O_4@SiO_2@CdS (Figure 2A) and CuS (Figure 2G). Also, the well-defined profile of the corresponding element was also exhibited (Figure 2). These further indicate the core−shell−shell structured Fe_3O_4@SiO_2@CdS and CuS hollow microsphere have been successfully prepared. Also, the structures of the above-mentioned two species have been confirmed by X-ray diffraction (XRD) (Figure S1) and X-ray photoelectron spectroscopy (XPS) (Figure S2).

Entropy-Driven Mechanism and the Corresponding DNA Assembly. As shown in Scheme 1, the EDTD amplifier in this PEC system consists mainly of the ETC and FT modules. Without target miRNA-196a, the ETC and FT remain intact. Nevertheless, upon exposure to miRNA-196a, ETC could be dissociated into ET and the partially double-stranded DNA composite (CuS-P5/Fe_3O_4@SiO_2@CdS-P6/Target) in virtue of typical toehold-mediated strand displacement.[31] Additionally, once hybridized with FT, the above partially double-stranded DNA will be breathed from the middle single-strand DNA and promptly dissociated into CuS-P5/FT as the waste (W), Fe_3O_4@SiO_2@CdS-P6 for PEC signal acquisition, and the target for initiating the DNA circuit for the next round. After multiple rounds of signal amplification, a lot of Fe_3O_4@SiO_2@CdS-P6 composites are released, leading to the recovery of photocurrent which has been blocked by the CuS hollow spheres. Therefore, the total reaction for this entropy-driven process could be expressed in Figure 3A. To confirm the operation of the entropy-driven amplifier, the Gibbs free energy equation was shown as below.

$$\Delta G = \Delta H - T\Delta S \quad (1)$$

ΔH and ΔS denote the changes in enthalpy and entropy in the system, respectively. T expresses the thermodynamic temperature. The total number of base pairs and complementary chains remained constant before and after the reaction, giving $\Delta H \approx 0$. Thus, $T\Delta S$ is the driving force that results from the liberated molecules in a thermodynamic entropy increasing system. Herein, the Gibbs free energy change can be described as eq 2.

https://dx.doi.org/10.1021/acsnano.0c09374
ACS Nano 2021, 15, 1710−1717

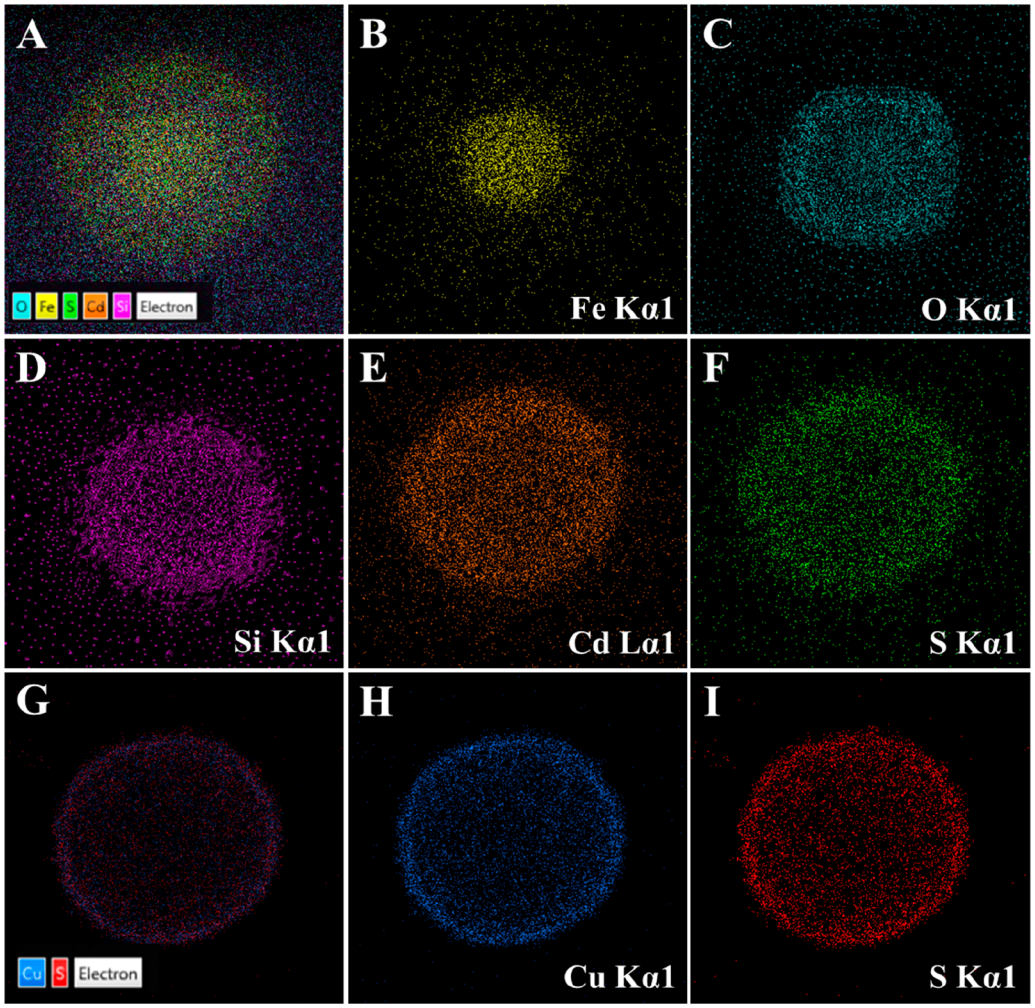

Figure 2. Elemental mappings of Fe (B), O (C), Si (D), Cd (E), and S (F) corresponding to Fe_3O_4@SiO_2@CdS (A) and elemental mappings of Cu (H) and S (I) corresponding to CuS (G).

$$\Delta G = \Delta G^0_W + \Delta G^0_{ET} + \Delta G^0_R - \Delta G^0_{ETC} - \Delta G^0_{FT} + RT \ln Q \quad (2)$$

In eq 2, Q refers to the reaction quotient and ΔG^0_X is the species X standard free energy, which can be worked out by free software NUPACK as below.

$$\Delta G^0_W + \Delta G^0_{ET} + \Delta G^0_R - \Delta G^0_{ETC} - \Delta G^0_{FT} = -0.33 \text{ kcal/mol} \quad (3)$$

Thus, when the reaction reaches equilibrium ($\Delta G = 0$), the Q value can be reckoned from eqs 2 and 3 to be 1.75. Also, Q can be expressed as eq 4.

$$Q = \frac{([W]/c^0)([ET]/c^0)([R]/c^0)}{([ETC]/c^0)([FT]/c^0)} \quad (4)$$

Herein, the original concentration of ETC and FT is 10 nmol L^{-1}, C^0 = 1 mol L^{-1}. Then, the ultimate concentration (x nmol L^{-1}) of R can be obtained by the following equation.

$$\frac{(10^{-9}x)^3}{[10^{-9}(10-x)]^2} = 1.75$$

Thus, the x value between 9.998 and 9.9998 nmol L^{-1} can be estimated by the bisection method, suggesting that the reaction conversion is more than 99.98% without consideration of the reaction time.

Native polyacrylamide gel electrophoresis (PAGE) was used to further evaluate the feasibility of an EDTD amplifier. As shown in Figure 3B, lanes 1−7 clearly show the single and assembled structures of strands P1−P7 based on the Watson−Crick base-pairing rule, respectively. As can be seen from lanes 6 and 7, the tetrahedron ETC and FT was successfully synthesized. As shown in lane 9, there is only a wide band appearing at the top, indicating that ETC and FT remain the same and do not cross-react. Upon exposure to target miRNA-196a, a toehold-mediated strand displacement reaction happened, resulting in the generation of ET and partially double-stranded DNA (lane 8). However, upon exposure to miRNA-196a and FT, the DNA-tetrahedral-nanostructure-based entropy increasing system was triggered, and strand P6 was released (lane 10). In short, the electrophoretic mobility decreased significantly with the molecular weight increasing or more complex spatial construction, while for those DNA tetrahedral nanostructures, the increase of DNA strands at the top branch nearly has no influence on the band position considering their relative small figures. This proves the successful preparation of DNA tetrahedral nanostructures and the effective and feasible entropy-driven DNA amplifier system.

https://dx.doi.org/10.1021/acsnano.0c09374
ACS Nano 2021, 15, 1710−1717

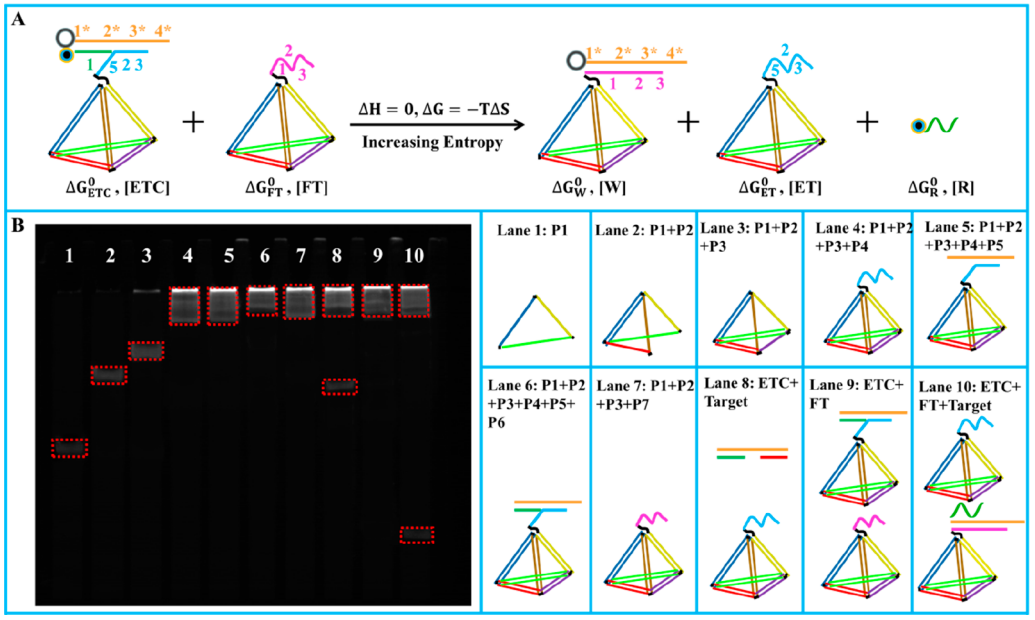

Figure 3. (A) Reaction equation of the DNA tetrahedral nanostructure-amplified system with thermodynamic parameters. (B) Native PAGE of the entropy increasing system. Lane 1: P1: 5 μmol L^{-1} × 5 μL; lane 2: P1 + P2: 5 μmol L^{-1} × 5 μL; lane 3: P1 + P2 + P3: 5 μmol L^{-1} × 5 μL; lane 4: P1 + P2 + P3 + P4: 5 μmol L^{-1} × 5 μL; lane 5: P1 + P2 + P3 + P4 + P5: 5 μmol L^{-1} × 5 μL; lane 6: P1 + P2 + P3 + P4 + P5 + P6: 5 μmol L^{-1} × 5 μL; lane 7: P1 + P2 + P3 + P7: 5 μmol L^{-1} × 5 μL; lane 8: ETC: 5 μmol L^{-1} × 5 μL + target: 5 μmol L^{-1} × 5 μL (0.004×); lane 9: ETC + FT: 5 μmol L^{-1} × 5 μL; lane 10: ETC + FT: 5 μmol L^{-1} × 5 μL + target: 5 μmol L^{-1} × 5 μL (0.004×).

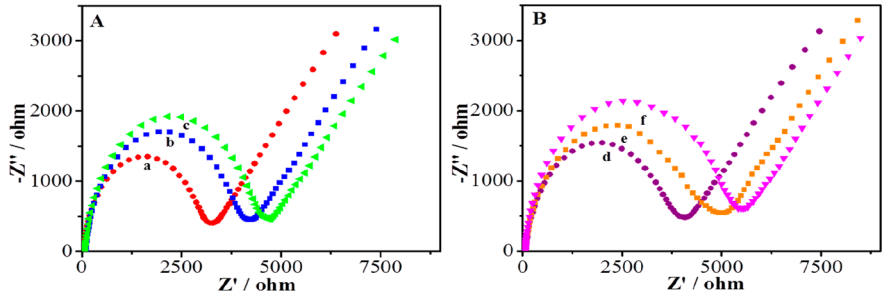

Figure 4. Electrochemical impedance spectroscopy of (a) Fe_3O_4@SiO_2@CdS, (b) Fe_3O_4@SiO_2@CdS-CS, (c) Fe_3O_4@SiO_2@CdS-P6, (d) CuS, (e) CuS-CS, and (f) CuS-P5 modified glassy carbon electrodes in 2.5 mmol L^{-1} $K_4Fe(CN)_6$ and $K_3Fe(CN)_6$ solution containing 0.2 mol L^{-1} KCl.

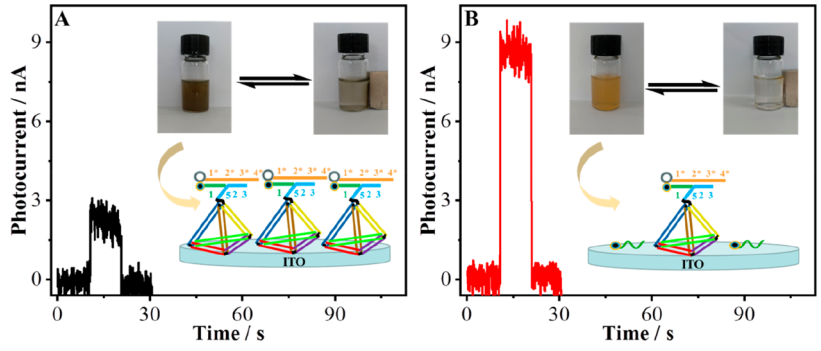

Figure 5. As-designed PEC biosensor performed in the absence (A) and presence (B) of 5 fmol L^{-1} miRNA-196a.

To affirm that the DNAs bind to Fe_3O_4@SiO_2@CdS and CuS particles, electrochemical impedance spectroscopy (EIS) was used to perform Nyquist plots for the readout of electron-transfer resistance (R_{ct}). As shown in Figure 4A, curve a shows the R_{ct} of 3336 Ω for Fe_3O_4@SiO_2@CdS particles. In contrast, the R_{ct} of curve b and curve c increases to 4250 and 4750 Ω, respectively. This suggests that chitosan (CS) and P6 were successfully bound to Fe_3O_4@SiO_2@CdS particles in order. It is the same case for CuS-P5 from Figure 4B. These could be explained by the insulator nature of CS and the anion polymer of DNA, which inhibited the electron transfer of the redox couple to the surface of modified GCE.

Analytical Performance. The EDTD amplifier coupled with a superparamagnetic-nanostructure-based PEC biosensor

https://dx.doi.org/10.1021/acsnano.0c09374
ACS Nano 2021, 15, 1710−1717

was applied for the measurement of miRNA-196a. Without the target, the ETC was extracted by magnetic separation and assembled on the ITO electrode, and a weak photocurrent of 2.72 nA was obtained (Figure 5A). Upon exposure to 5 fmol L^{-1} miRNA-196a, the DNA circuit is promptly initiated, and a certain amount of Fe_3O_4@SiO_2@CdS-P6 was released from ETC. Then, for the same reason, the remaining ETC and the released Fe_3O_4@SiO_2@CdS-P6 could be facilely extracted for the preparation of a photoanode, which shows an increased photocurrent of 9.71 nA (Figure 5B). Compared to the photocurrent increment in Figure 5, it can be concluded that CuS particles can effectively inhibit light from being absorbed by magnetic-optical Fe_3O_4@SiO_2@CdS particles (Figure S3). As shown in the insets of Figure 5, ETC and the liberated Fe_3O_4@SiO_2@CdS-P6 can be extracted by magnetic separation in several seconds and uniformly redispersed in the aqueous phase, suggesting the superparamagnetic feature of Fe_3O_4@SiO_2@CdS particles.[32] Also, compared to the color of the composite in the inset of Figure 5A, the color of the inset in Figure 5B changes from dark to light brown, indicating that partial dark CuS-P5 was liberated from ETC with the trigger of 5 fmol L^{-1} miRNA-196a. Based on this strategy of an EDTD amplifier coupled with superparamagnetic nanostructures, the fabricated PEC biosensor is promising to monitor miRNA-196a.

As can be seen from Figure 6A, the photocurrent enhances with the concentration of miRNA-196a improvement. Also,

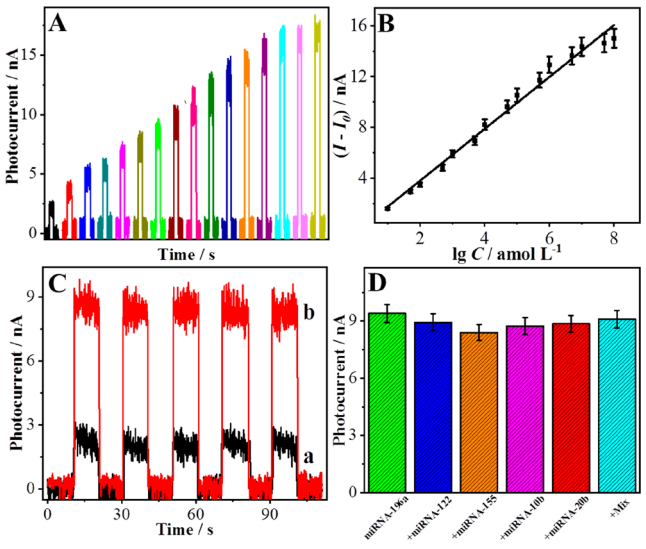

Figure 6. (A) The as-designed PEC biosensor performed in the presence of 0, 0.01, 0.05, 0.1, 0.5, 1, 5, 10, 50, 100, 500, 1000, 5000, 10,000, 50,000, and 100,000 fmol mL^{-1} miRNA-196a at a bias of 0.1 V with chopped light irradiation. (B) Corresponding calibration curve. (C) Photocurrents of the PEC biosensor in the absence (a) and presence (b) of 5 fmol L^{-1} miRNA-196a with five consecutive irradiations. (D) The effects of miRNA-122 (200-fold), miRNA-155 (200-fold), miRNA-10b (200-fold), miRNA-20b (200-fold), and the mixture (each 50-fold) on the photocurrent measurement in the presence of 5 fmol L^{-1} miRNA-196a.

the dynamic linear range between photocurrent increment and log *C* ranging from 10 amol L^{-1} to 10 pmol L^{-1} can be inferred from the calibration curve (Figure 6B). The detection limit of 3.1 amol L^{-1} (3S/N) could be worked out, and it is advantageous over all of the reported approaches for miRNA-196a (see Table S2) as far as we know. Also, such a low limit of detection is superior to that of other miRNA assay methods such as electrochemical[33,34] (53 and 100 amol L^{-1}), fluorescence[35,36] (72 pmol L^{-1}, 44 fmol L^{-1}), ECL[37] (9.4 amol L^{-1}), and PEC[38−40] (0.29, 0.47, and 0.13 fmol L^{-1}). Such an excellent sensitivity can be attributed to the DNA-tetrahedron-based entropy-driven amplifier, the efficient enrichment and extraction of the superparamagnetic nanomaterials functionalized with signal DNA, the "signal-on" type design, and the intrinsic ultrasensitivity of PEC sensing with low background noise. Also, this PEC biosensor has additional advantages of efficient electrode fabrication and expanded linear range, which are also comparable to or even superior to other detection methods (see Table S2).

Stability and selectivity are important parameters that have been evaluated for the prepared PEC biosensor (Figure 6C,D). As shown in Figure 6C, upon exposure to 0 and 5 fmol L^{-1} miRNA-196a, the five consecutive photocurrents based on the modified ITO electrodes (curves a and b) almost remain unchanged, suggesting the fabricated PEC biosensor is robust. Besides, the shelf time of the PEC sensor was assessed by the photocurrent measurement over 4 weeks. The results show that the output signal remains almost unchanged within 2 weeks, and the signal can still reach the initial level of 95.4% after 4 weeks, indicating that the PEC biosensor can retain the stability for a long time (Figure S4). Also, the relative standard deviation (RSD) of 5.2% for the six freshly prepared PEC biosensors calculated from the calibration curve indicated that the PEC sensor is reproductive (Figure 6B). This reproducibility is almost comparable to those of other detection methods (see Table S3). Additionally, the specificity of PEC biosensors was assessed by adding conventional species such as miRNA-122, miRNA-155, miRNA-10b, and miRNA-20b and their mixtures to 5 fmol L^{-1} miRNA-196a. As can be seen from Figure 6D, the maximum interference was less than 7.3%, even if 200-fold each miRNA and a mixture of these species (each 50-fold) were introduced. This result indicates the PEC biosensor has excellent specificity to the target miRNA-196a over its analogues (see Table S3). Herein, except for the magnetic separation effect on its selectivity, the molecular engineering of an exclusive EDTD amplifier shows increased mechanical rigidity and biostability compared to other structured entropy-driven strategies, improving the hybridization efficiency and also the reaction specificity.

The PEC assay with the spiked method was utilized to assess the reliability of the PEC biosensor in practical settings. As shown in Table S4, the recovery ranges from 96.4 to 104.3% and the RSD is less than 3.62%; also, the detection results have been confirmed by Northern blotting as the standard method, indicating that the PEC biosensor has excellent accuracy and precision and is competent for monitoring miRNA-196a in human serum samples.

CONCLUSIONS

In brief, a split-mode and signal-on PEC biosensor for miRNA-196a was constructed by an EDTD amplifier integrated to biofunctionalized superparamagnetic nanoarchitectures. The THD has good performance in mechanical rigidity and structural stability, which are in favor of precise identification units and specific orientations and benefited to enhance the selectivity. The strategy based on EDTD amplification has the advantages of no enzyme participation, simple program, low cost, as well as easy design and modification. Moreover, superparamagnetic nanostructures contribute to the split-mode

https://dx.doi.org/10.1021/acsnano.0c09374
ACS Nano 2021, 15, 1710−1717

PEC biosensor and address the shortcoming in limited specificity for the most conventional sensors by removing the coexisting species from a complex solution matrix or modified electrode surfaces. Besides the excellent specificity, this exquisite and split-mode PEC biosensor is competent for the monitoring of miRNA-196a in practical settings with other good performance in ultrasensitivity, efficient electrode fabrication, stability, and reproducibility. This strategy provides a reliable solution for the design of high-performance PEC biosensors.

METHODS

Preparation of PEC Biosensor. Typically, 0.5 mL of Fe_3O_4@SiO_2@CdS suspension was scattered into 2 mL of 0.1 wt % chitosan in acetic acid solution and heated for 2 h at 50 °C. After magnetic extraction and wash treatment, the composite of Fe_3O_4@SiO_2@CdS-NH_2 was obtained. Meanwhile, 100 μL of 2 μmol L^{-1} annealed DNA of P6 was introduced to 1.5 mL Tris−HCl buffered solution containing 400 μL of EDC/NHS solution (0.1 mol L^{-1}) and reacted for 3 h at 25 °C to activate the carboxyl in P6. Next, the prepared Fe_3O_4@SiO_2@CdS-NH_2 composite was introduced and stirred for 4 h at 25 °C for the generation of Fe_3O_4@SiO_2@CdS-P6 composite.

Also, 1 mL of CuS hollow microsphere suspension was added into 3 mL of 0.1 wt % chitosan in acetic acid solution. After vigorously stirring for 2 h at 25 °C, the resulting composite was collected by centrifugation and washed several times with water, and then, it was scattered into 3 mL of 5% glutaric dialdehyde solution and heated at 37 °C for 1 h. After centrifugation and wash treatment for several times with water, 100 μL of 2 μmol L^{-1} annealed DNA of P5 tagged with an amino group was added and incubated at 4 °C overnight. After centrifugation and water washing steps, the conjugate of CuS-P5 was obtained. Then, the equimolar amount of Fe_3O_4@SiO_2@CdS-P6 (signal DNA strand), CuS-P5 (block DNA strand), and entropy beacon tetrahedron (ET) were added into 2 mL of Tris−HCl buffer and incubated for 2 h at 37 °C to form the three-strand-structured ET composite (ETC) after washing by Tris−HCl buffered solution with the assistance of magnetic extraction. Then, a certain concentration of miRNA-196a was introduced in 200 μL of Tris−HCl buffered solution containing 2 μmol L^{-1} ETC and fuel tetrahedron (FT). After incubation for 3 h at 25 °C, the resulting product and byproduct were separated by magnetic extraction and washed several times, and then, they were redispersed in 40 μL of Tris−HCl buffered solution. Subsequently, 20 μL of Fe_3O_4@SiO_2@CdS-P6 with different concentrations and unreacted ETC suspension was cast on a cleaned ITO electrode and dried at 25 °C, and then, the photoanode was successfully fabricated. Further, the photoelectric response was read out in pure PBS (pH 7.0). The monitor of miRNA-196a in practical settings was also performed with the same approach except for utilizing the human serum samples instead of the miRNA-196a standard solution.

ASSOCIATED CONTENT

Supporting Information

The Supporting Information is available free of charge at https://pubs.acs.org/doi/10.1021/acsnano.0c09374.

The reagents and apparatus, the synthesis of Fe_3O_4 colloidal nanocrystal clusters, Fe_3O_4@SiO_2 particles, Fe_3O_4@SiO_2@CdS particles, and CuS hollow microspheres, the preparation and characterization of ET and FT modules, the test results and their performance comparisons (Tables S2−S4), and other partial characterizations (Figures S1−S4) (PDF)

AUTHOR INFORMATION

Corresponding Authors

Hongbo Li − *School of Chemistry and Chemical Engineering, Yancheng Institute of Technology, Yancheng 224051, PR China*; orcid.org/0000-0001-8662-0427; Phone: +86-515-88298735; Email: hbli@ycit.edu.cn

Jing Li − *School of Chemistry and Chemical Engineering, Yancheng Institute of Technology, Yancheng 224051, PR China*; Phone: +86-515-88298735; Email: jli@ycit.edu.cn

Authors

Min Han − *School of Chemistry and Chemical Engineering, Yancheng Institute of Technology, Yancheng 224051, PR China*

Xuan Weng − *School of Chemistry and Chemical Engineering, Yancheng Institute of Technology, Yancheng 224051, PR China*

Yuye Zhang − *School of Chemistry and Chemical Engineering, Yancheng Institute of Technology, Yancheng 224051, PR China*

Complete contact information is available at: https://pubs.acs.org/10.1021/acsnano.0c09374

Notes

The authors declare no competing financial interest.

ACKNOWLEDGMENTS

We acknowledge the financial support from the Natural Science Foundation of China (21505117, 21775135) and the Natural Science Foundation of Jiangsu Province (BK20161309, BK20201473), and this work was also sponsored by Qinglan Project of Jiangsu Province.

REFERENCES

(1) Li, Z.; Zhao, B.; Wang, D.; Wen, Y.; Liu, G.; Dong, H.; Song, S.; Fan, C. DNA Nanostructure-Based Universal Microarray Platform for High-Efficiency Multiplex Bioanalysis in Biofluids. *ACS Appl. Mater. Interfaces* **2014**, *6*, 17944−17953.

(2) Xiao, M.; Lai, W.; Man, T.; Chang, B.; Li, L.; Chandrasekaran, A. R.; Pei, H. Rationally Engineered Nucleic Acid Architectures for Biosensing Applications. *Chem. Rev.* **2019**, *119*, 11631−11717.

(3) Huang, J.; Yang, X. H.; He, X. X.; Wang, K. M.; Liu, J. B.; Shi, H.; Wang, Q.; Guo, Q. P.; He, D. G. Design and Bioanalytical Applications of DNA Hairpin-Based Fluorescent Probes. *TrAC, Trends Anal. Chem.* **2014**, *53*, 11−20.

(4) Deng, C.; Pi, X.; Qian, P.; Chen, X.; Wu, W.; Xiang, J. High-Performance Ratiometric Electrochemical Method Based on the Combination of Signal Probe and Inner Reference Probe in One Hairpin-Structured DNA. *Anal. Chem.* **2017**, *89*, 966−973.

(5) Nie, J.; Zhang, D. W.; Tie, C.; Zhou, Y. L.; Zhang, X. X. A Label-Free DNA Hairpin Biosensor for Colorimetric Detection of Target with Suitable Functional DNA Partners. *Biosens. Bioelectron.* **2013**, *49*, 236−242.

(6) Miao, P.; Tang, Y. G. Dumbbell Hybridization Chain Reaction Based Electrochemical Biosensor for Ultrasensitive Detection of Exosomal miRNA. *Anal. Chem.* **2020**, *92*, 12026−12032.

(7) Karunanayake Mudiyanselage, A. P. K. K.; Yu, Q.; Leon-Duque, M. A.; Zhao, B.; Wu, R.; You, M. Genetically Encoded Catalytic Hairpin Assembly for Sensitive RNA Imaging in Live Cells. *J. Am. Chem. Soc.* **2018**, *140*, 8739−8745.

(8) Li, D.; Zhang, T.; Yang, F.; Yuan, R.; Xiang, Y. Efficient and Exponential Rolling Circle Amplification Molecular Network Leads to Ultrasensitive and Label-Free Detection of MicroRNA. *Anal. Chem.* **2020**, *92*, 2074−2079.

(9) Choi, H. M. T.; Schwarzkopf, M.; Fornace, M. E.; Acharya, A.; Artavanis, G.; Stegmaier, J.; Cunha, A.; Pierce, N. A. Third-Generation *in Situ* Hybridization Chain Reaction: Multiplexed, Quantitative, Sensitive, Versatile, Robust. *Development* **2018**, *145*, dev165753.
(10) Lin, M.; Song, P.; Zhou, G.; Zuo, X.; Aldalbahi, A.; Lou, X.; Shi, J.; Fan, C. Electrochemical Detection of Nucleic Acids, Proteins, Small Molecules and Cells Using a DNA-Nanostructure-Based Universal Biosensing Platform. *Nat. Protoc.* **2016**, *11*, 1244−1263.
(11) Ozhalici-Unal, H.; Armitage, B. A. Fluorescent DNA Nanotags Based on a Self-Assembled DNA Tetrahedron. *ACS Nano* **2009**, *3*, 425−433.
(12) He, L.; Lu, D.; Liang, H.; Xie, S.; Zhang, X.; Liu, Q.; Yuan, Q.; Tan, W. mRNA-Initiated, Three-Dimensional DNA Amplifier Able to Function inside Living Cells. *J. Am. Chem. Soc.* **2018**, *140*, 258−263.
(13) Ge, Z. L.; Pei, H.; Wang, L. H.; Song, S. P.; Fan, C. H. Electrochemical Single Nucleotide Polymorphisms Genotyping on Surface Immobilized Three-Dimensional Branched DNA Nanostructure. *Sci. China: Chem.* **2011**, *54*, 1273−1276.
(14) Wang, Z. G.; Xue, Q. W.; Tian, W. Z.; Wang, L.; Jiang, W. Quantitative Detection of Single DNA Molecules on DNA Tetrahedron Decorated Substrates. *Chem. Commun.* **2012**, *48*, 9661−9663.
(15) Su, J.; Wu, F. B.; Xia, H. P.; Wu, Y. F.; Liu, S. Q. Accurate Cancer Cell Identification and MicroRNA Silencing Induced Therapy Using Tailored DNA Tetrahedron Nanostructures. *Chem. Sci.* **2020**, *11*, 80−86.
(16) Zhou, Z. X.; Sohn, Y. S.; Nechushtai, R.; Willner, I. DNA Tetrahedra Modules as Versatile Optical Sensing Platforms for Multiplexed Analysis of miRNAs, Endonucleases, and Aptamer-Ligand Complexes. *ACS Nano* **2020**, *14*, 9021−9031.
(17) Fu, X. Y.; Ke, G. L.; Peng, F. Q.; Hu, X.; Li, J. Q.; Shi, Y. Y.; Kong, G. Z.; Zhang, X. B.; Tan, W. H. Size-Selective Molecular Recognition Based on a Confined DNA Molecular Sieve Using Cavity-Tunable Framework Nucleic Acids. *Nat. Commun.* **2020**, *11*, 1518.
(18) Wang, S.; Zhang, L. Q.; Wan, S.; Cansiz, S.; Cui, C.; Liu, Y.; Cai, R.; Hong, C. Y.; Teng, I. T.; Shi, M. L.; Wu, Y.; Dong, Y. Y.; Tan, W. H. Aptasensor with Expanded Nucleotide Using DNA Nanotetrahedra for Electrochemical Detection of Cancerous Exosomes. *ACS Nano* **2017**, *11*, 3943−3949.
(19) Ma, X. Y.; Miao, P. Silver Nanoparticle@DNA Tetrahedron-Based Colorimetric Detection of HIV-Related DNA with Cascade Strand Displacement Amplification. *J. Mater. Chem. B* **2019**, *7*, 2608−2612.
(20) Fan, Z. Q.; Lin, Z. Q.; Wang, Z. P.; Wang, J. F.; Xie, M. H.; Zhao, J. F.; Zhang, K.; Huang, W. Dual-Wavelength Electrochemiluminescence Ratiometric Biosensor for NF-kappa B p50 Detection with Dimethylthiodiaminoterephthalate Fluorophore and Self-Assembled DNA Tetrahedron Nanostructures Probe. *ACS Appl. Mater. Interfaces* **2020**, *12*, 11409−11418.
(21) Li, M.; Xiong, C.; Zheng, Y.; Liang, W.; Yuan, R.; Chai, Y. Ultrasensitive Photoelectrochemical Biosensor Based on DNA Tetrahedron as Nanocarrier for Efficient Immobilization of CdTe QDs-Methylene Blue as Signal Probe with Near-Zero Background Noise. *Anal. Chem.* **2018**, *90*, 8211−8216.
(22) Lin, S.; Gregory, R. I. MicroRNA Biogenesis Pathways in Cancer. *Nat. Rev. Cancer* **2015**, *15*, 321−333.
(23) Lu, J.; Getz, G.; Miska, E. A.; Alvarez-Saavedra, E.; Lamb, J.; Peck, D.; Sweet-Cordero, A.; Ebert, B. L.; Mak, R. H.; Ferrando, A. A.; Downing, J. R.; Jacks, T.; Horvitz, H. R.; Golub, T. R. MicroRNA Expression Profiles Classify Human Cancers. *Nature* **2005**, *435*, 834−838.
(24) Streit, S.; Michalski, C. W.; Erkan, M.; Kleeff, J. R.; Friess, H. Northern Blot Analysis for Detection and Quantification of RNA in Pancreatic Cancer Cells and Tissues. *Nat. Protoc.* **2009**, *4*, 37−43.
(25) Shlyapnikov, Y. M.; Malakhova, E. A.; Shlyapnikova, E. A. Rapid Amplification-Free Microarray-Based Ultrasensitive Detection of DNA. *Anal. Chem.* **2019**, *91*, 11209−11214.
(26) Thomou, T.; Mori, M. A.; Dreyfuss, J. M.; Konishi, M.; Sakaguchi, M.; Wolfrum, C.; Rao, T. N.; Winnay, J. N.; Garcia-Martin, R.; Grinspoon, S. K. Adipose-Derived Circulating miRNAs Regulate Gene Expression in Other Tissues. *Nature* **2017**, *542*, 450−455.
(27) Ding, J. H.; Ma, C. J.; Chen, M. Y.; Chen, B.; Yuan, B. F.; Feng, Y. Q. Quantification and Single-Base Resolution Analysis of N1-Methyladenosine in mRNA by Ligation-Assisted Differentiation. *Anal. Chem.* **2020**, *92*, 2612−2619.
(28) Zhang, D. Y.; Turberfield, A. J.; Yurke, B.; Winfree, E. Engineering Entropy-Driven Reactions and Networks Catalyzed by DNA. *Science* **2007**, *318*, 1121−1125.
(29) Zhang, N.; Shi, X. M.; Guo, H. Q.; Zhao, X. Z.; Zhao, W. W.; Xu, J. J.; Chen, H. Y. Gold Nanoparticle Couples with Entropy-Driven Toehold-Mediated DNA Strand Displacement Reaction on Magnetic Beads: Toward Ultrasensitive Energy-Transfer-Based Photoelectrochemical Detection of miRNA-141 in Real Blood Sample. *Anal. Chem.* **2018**, *90*, 11892−11898.
(30) Masud, M. K.; Na, J.; Younus, M.; Hossain, M. S. A.; Bando, Y.; Shiddiky, M. J. A.; Yamauchi, Y. Superparamagnetic Nanoarchitectures for Disease-Specific Biomarker Detection. *Chem. Soc. Rev.* **2019**, *48*, 5717−5751.
(31) Lv, Y.; Cui, L.; Peng, R.; Zhao, Z.; Qiu, L.; Chen, H.; Jin, C.; Zhang, X. B.; Tan, W. Entropy Beacon: A Hairpin-Free DNA Amplification Strategy for Efficient Detection of Nucleic Acids. *Anal. Chem.* **2015**, *87*, 11714−11720.
(32) Li, J.; Xu, L.; Shen, Y.; Guo, L.; Yin, H.; Fang, X.; Yang, Z.; Xu, Q.; Li, H. Superparamagnetic Nanostructures for Split-Type and Competitive-Mode Photoelectrochemical Aptasensing. *Anal. Chem.* **2020**, *92*, 8607−8613.
(33) Guo, Q.; Yu, Y.; Zhang, H.; Cai, C.; Shen, Q. Electrochemical Sensing of Exosomal MicroRNA Based on Hybridization Chain Reaction Signal Amplification with Reduced False-Positive Signals. *Anal. Chem.* **2020**, *92*, 5302−5310.
(34) Masud, M. K.; Na, J.; Lin, T.-E.; Malgras, V.; Preet, A.; Ibn Sina, A. A.; Wood, K.; Billah, M.; Kim, J.; You, J.; Kani, K.; Whitten, A. E.; Salomon, C.; Nguyen, N.-T.; Shiddiky, M. J. A.; Trau, M.; Hossain, M. S. A.; Yamauchi, Y. Nanostructured Mesoporous Gold Biosensor for MicroRNA Detection at Attomolar Level. *Biosens. Bioelectron.* **2020**, *168*, 112429.
(35) Liu, Y.; Shen, T.; Li, J.; Gong, H.; Chen, C.; Chen, X.; Cai, C. Ratiometric Fluorescence Sensor for the MicroRNA Determination by Catalyzed Hairpin Assembly. *ACS Sens.* **2017**, *2*, 1430−1434.
(36) Tang, Y.; Liu, M.; Zhao, Z.; Li, Q.; Liang, X.; Tian, J.; Zhao, S. Fluorometric Determination of MicroRNA-122 by Using ExoIII-Aided Recycling Amplification and Polythymine Induced Formation of Copper Nanoparticles. *Microchim. Acta* **2019**, *186*, 133.
(37) Huo, X.-L.; Zhang, N.; Yang, H.; Xu, J.-J.; Chen, H.-Y. Electrochemiluminescence Resonance Energy Transfer System for Dual-Wavelength Ratiometric miRNA Detection. *Anal. Chem.* **2018**, *90*, 13723−13728.
(38) Hao, N.; Lu, J.; Chi, M.; Xiong, M.; Zhang, Y.; Hua, R.; Wang, K. A Universal Photoelectrochemical Biosensor for Dual MicroRNA Detection Based on Two CdTe Nanocomposites. *J. Mater. Chem. B* **2019**, *7*, 1133−1141.
(39) Li, B.; Yin, H.; Zhou, Y.; Wang, M.; Wang, J.; Ai, S. Photoelectrochemical Detection of miRNA-319a in Rice Leaf Responding to Phytohormones Treatment Based on CuO-$CuWO_4$ and Rolling Circle Amplification. *Sens. Actuators, B* **2018**, *255*, 1744−1752.
(40) Wang, M.; Yin, H.; Zhou, Y.; Sui, C.; Wang, Y.; Meng, X.; Waterhouse, G. I. N.; Ai, S. Photoelectrochemical Biosensor for MicroRNA Detection Based on a MoS_2/g-C_3N_4/Black TiO_2 Heterojunction with Histostar@AuNPs for Signal Amplification. *Biosens. Bioelectron.* **2019**, *128*, 137−143.

https://dx.doi.org/10.1021/acsnano.0c09374
ACS Nano 2021, 15, 1710−1717